Research Square

Preprints are preliminary reports that have not undergone peer review.
They should not be considered conclusive, used to inform clinical practice,
or referenced by the media as validated information.

Longitudinal Percentage Change in DTI-ALPS and MMSE as Joint Markers of MCI-to-Alzheimer's Disease Conversion

Rutuja Ingavale
Manipal Institute of Technology, Manipal Academy of Higher Education
Haripriya S
Manipal Institute of Technology, Manipal Academy of Higher Education
Amritanshu Gupta
amritanshu.gupta@manipal.edu

Manipal Institute of Technology, Manipal Academy of Higher Education

Article

Keywords: DTI-ALPS, Glymphatic System, Alzheimer’s Disease, Mild Cognitive Impairment, Longitudinal Biomarkers, MMSE Decline

Posted Date: November 5th, 2026

DOI: https://doi.org/10.21203/rs.3.rs-10662564/v1

License: This work is licensed under a Creative Commons Attribution 4.0 International License.
Read Full License

Additional Declarations: No competing interests reported.

Longitudinal Percentage Change in DTI-ALPS and MMSE as Joint Markers of MCI-to-Alzheimer's Disease Conversion

Rutuja Ingavale[1], Haripriya S[1] and Amritanshu Gupta[1]*

[1] School of Electrical Engineering, Manipal Institute of Technology, Manipal Academy of Higher Education, Manipal, India

***Corresponding author**
Amritanshu Gupta
School of Electrical Engineering,
Manipal Institute of Technology,
Manipal Academy of Higher Education,
Manipal – 576104
Karnataka
Email: amritanshu.gupta@manipal.edu
ORCID: 0000-0003-0437-5371

Abstract

Early Alzheimer's disease prediction remains an open challenge. DTI-ALPS, an imaging-derived marker of glymphatic clearance, has been proposed as an earlier signal, but absolute ALPS values overlap substantially across diagnostic groups, limiting their value as single-timepoint measurements. This study examined whether longitudinal percentage change in DTI-ALPS from baseline, rather than a single absolute value, better distinguishes subjects who remain stable from those who convert from MCI to Alzheimer's disease, and whether combining it with longitudinal MMSE change adds further value. Unlike prior work linking baseline ALPS to later outcomes, we used ADNI data to compare Stable MCI and MCI-to-AD subjects using longitudinal percentage changes in ALPS and MMSE from each subject's own baseline. Overcoming the overlap inherent to absolute baseline ALPS, both measures differed significantly, showing medium and large effect sizes for ALPS and MMSE changes, and were only weakly and non-significantly correlated with each other. A logistic regression combining them did not significantly outperform MMSE alone on classification accuracy, but ALPS change remained an independent, significant predictor after MMSE was accounted for, indicating that glymphatic decline carries conversion-relevant information of its own. Together, these results support tracking change from an individual's own baseline when assessing early Alzheimer's risk with DTI-ALPS.

Keywords: DTI-ALPS; Glymphatic System; Alzheimer’s Disease; Mild Cognitive Impairment; Longitudinal Biomarkers; MMSE Decline

1. Introduction

Alzheimer’s disease (AD) is projected to affect roughly 153 million people worldwide by 2050. This is more than double the 2019 estimate (Nichols et al., 2022). AD is usually recognised only once cognitive symptoms are already noticeable or advanced, and by then the underlying neurodegenerative process has often been running for years. This is part of why the field has shifted toward staging Alzheimer’s by its underlying biology rather than symptoms alone, an approach formalised in the NIA-AA Research Framework’s amyloid/tau/neurodegeneration scheme. The goal is to catch the disease earlier, while it is still preclinical or prodromal, when there may still be room to change its course. This requires a different kind of marker. Rather than simply flagging that the disease is present, it has to track how a person is changing over time, since a single measurement only tells you whether a person is sick or healthy once symptoms have already manifested. This study examines one such pair of candidate markers in a retrospective, longitudinal analysis of the Alzheimer’s Disease Neuroimaging Initiative (ADNI), an existing multi-site imaging and cognitive dataset rather than a newly collected cohort.

The first of these two markers comes from a comparatively recent line of work on the brain’s glymphatic system (Iliff et al., 2012, 2013). This is a perivascular network that clears metabolic waste, including amyloid-β, by exchanging cerebrospinal fluid with interstitial fluid, and in animal models, it accounts for more than half of the brain’s amyloid-β clearance. Sleep is closely tied to this clearance process as well. In mice, natural sleep and anaesthesia caused the interstitial space to expand and amyloid-β clearance to increase along with it (Xie et al., 2013). Later work extended this connection to human dementia. As glymphatic function declines with

age and sleep becomes more fragmented, the two may combine into a shared pathway running across several neurodegenerative diseases rather than being specific to Alzheimer's alone (Nedergaard & Goldman, 2020). If this clearance system breaks down, the proteins central to Alzheimer's pathology may build up faster than they otherwise would. That is part of why glymphatic dysfunction is thought to come before, and possibly help forecast, the cognitive decline that appears later on. Measuring this pathway directly in humans is not straightforward, though DTI-ALPS (Diffusion Tensor Image Analysis Along the Perivascular Space) offers one non-invasive route in, using diffusivity along perivascular spaces relative to fiber-crossing directions as a proxy for glymphatic activity (Taoka et al., 2017). This isn't just a theoretical proxy either. A study using intrathecal contrast tracing found that the ALPS index correlates with directly measured glymphatic clearance (Zhang et al., 2021). DTI-ALPS has been used across the whole range from mild cognitive impairment to established Alzheimer's disease. Further, in one well-powered study spanning three diagnostic groups, ALPS values came out lower in AD than in healthy controls, and those lower values also went along with greater amyloid burden and reduced glucose metabolism on PET (Kamagata et al., 2022).

Applying DTI-ALPS to a diagnostic question runs into a problem that shows up repeatedly in this literature. A single ALPS reading, taken at a single point in time, doesn't cleanly separate people by diagnosis. Findings across cohorts don't line up well either. Some studies only detect a significant group difference after adjusting for age, and even then, only in one hemisphere(Steward et al., 2021). Guo and colleagues' own two-cohort design illustrates this. They reported a significant difference between cognitively normal and MCI groups in their ADNI sample, but that difference did not reach significance in their second, independent cohort (Guo et al., 2025). And even when a difference does turn out significant, it tends to be small (Kamagata et al., 2022), which in practice means a lot of overlap between people who will eventually develop AD and people who won't.

None of these points to a flaw in any one study. It more likely comes down to how much people genuinely differ from each other in baseline glymphatic function, shaped by age, vascular health, sleep, and anatomy, so the same ALPS number can mean quite different things depending on whose brain it came from. Given this degree of inter-individual variability at baseline, the more informative signal may not be a person's ALPS index at a single time point, but the magnitude of change from their own starting value. This shift in framing, from a single absolute measurement to a within-subject change score, is the central premise underlying this study. We test it directly, first by examining the overlap in baseline ALPS values within our own cohort, before turning to change-based measures. This approach depends on longitudinal DTI-ALPS change being a reliable signal in the first place, which reproducibility work supports under consistent imaging conditions (Taoka et al., 2022).

DTI-ALPS, as described above, is a direct imaging measurement of a specific physiological process, perivascular fluid clearance, not something inferred from behaviour. Cognitive trajectory works differently. It measures or estimates the downstream, accumulated effect of whatever is driving decline, without pointing to any one cause. That's part of why the two are worth pairing: one is tied closely to the underlying biology, the other to what a person's day-to-day functioning actually looks like, and they're unlikely to be picking up exactly the same thing at exactly the same time. The Mini-Mental State Examination (Folstein et al., 1975) fits naturally into this as a longitudinal marker. Work tracking MMSE over several years in MCI

cohorts has found distinct patterns of decline that predict how people go on to do cognitively, using the rate of change rather than a single starting score (Xie et al., 2013).

How these two markers relate to each other has itself become a focus of recent research. Guo et al. (2025) drew on two separate datasets, ADNI and an independent Chinese cohort, and found that a lower ALPS index at a single baseline scan predicted both faster MMSE decline down the line and a higher chance of converting from MCI to AD. In effect, ALPS was treated as a fixed risk marker, one reading taken early that forecasts what happens later on an entirely different measure. Another ADNI-based study found much the same thing, with baseline ALPS predicting later rates of amyloid buildup, brain atrophy, and cognitive decline, which places glymphatic impairment as an early event that comes before, and seems to forecast, what follows (Huang et al., 2024).

Guo and Huang's studies are really asking the same underlying question: whether an early snapshot can predict a later outcome. That's different from what motivates the present study. Here, both markers are expressed not as absolute scores but as percentage change from each subject's own baseline, and the question is whether these two change scores move together over time rather than whether one baseline value predicts the other's future. If a single ALPS measurement is compromised by the inter-subject variability discussed above, a baseline value predicting a future outcome carries that same weakness with it, however useful it turns out to be in practice. What hasn't been tested, as far as we know, is whether pairing percentage change in ALPS with percentage change in MMSE, rather than pairing a physiological baseline with a cognitive trajectory, adds anything beyond what either offers alone.

Work that has tried to combine imaging with cognitive markers to predict MCI-to-AD conversion doesn't point in one direction. Some studies, pairing structural MRI with cognitive testing and risk-factor measures, have done well at this (Devanand et al., 2007, 2008). One of them found that five early markers together were genuinely more useful than age and MMSE on their own. Other work pulls the other way. Combined models don't always beat the best single marker, and in some cases, cognitive scores alone did just as well as far more complicated combinations (Ewers et al., 2012; Gomar, 2011). Guo and colleagues sit somewhere in between, though their work rests entirely on baseline values rather than change over time. Taken together, these results hint that the benefit of combining markers may hinge less on combining them at all than on what exactly gets combined, baseline values, trajectories, or some mix of the two, which is exactly what this study tests directly, using percentage change from baseline for both markers instead of a baseline value for either.

Testing this needs repeated imaging and cognitive data from the same subjects over time, which is why we turned to ADNI. The dataset spans multiple phases and sites, following people over time as they move across the cognitively normal, MCI, and AD spectrum, using protocols that have stayed standardised for two decades of data collection (Arani et al., 2024; Jack et al., 2008; Petersen et al., 2010; Weiner et al., 2017). Its scale and long follow-up windows make it possible to compute within-subject change over meaningful stretches of time, a requirement of the argument above rather than a convenience of the dataset. Conversion here means a documented change in diagnosis from MCI to AD dementia at any point during follow-up, in accordance with ADNI's established diagnostic criteria.

This study has three aims: to test whether percentage change in the DTI-ALPS index from baseline separates stable and converting subjects better than absolute ALPS values do, to check whether longitudinal MMSE change shows the same pattern, and to ask whether change in the two measures is related, with ALPS change telling us something about conversion risk that MMSE change alone does not. In doing this, what we're really asking is whether a person's risk of progressing from MCI to Alzheimer's disease shows up more clearly not in a single glymphatic or cognitive measurement, but in how much that measurement changes from their baseline visit to the years that follow.

2. Methodology

This study investigated longitudinal changes in the DTI-ALPS index by comparing the baseline scan and the last available scan for each subject. Longitudinal changes were evaluated using two primary variables: the percentage change in the DTI-ALPS index from baseline, which quantified changes in glymphatic function, and the percentage change in the Mini-Mental State Examination (MMSE) score from baseline, which assessed changes in cognitive performance. Because the time interval between the baseline and last available scans differed across subjects, annualized percentage changes in both the DTI-ALPS index and MMSE score were also calculated.

The proposed pipeline is based on the framework described by Nakaya et al. (2025) but differs in several methodological aspects. Image registration is performed using the `dipy.align` module through a four-stage translation-rigid-affine-SDR pipeline instead of `FSL FLIRT/FNIRT`, which does not require administrator privileges on Windows. Registration quality is assessed for each subject by calculating the structural similarity index (SSIM) between the registered image and the FMRIB58 template, in addition to visual inspection. An automated slice-by-slice hole-filling correction is applied to the brain mask, addressing enclosed interior holes produced by `median_otsu() function` in some subjects. This helps in preserving the outer boundary of the brain mask generated by Otsu thresholding, along with restoring the enclosed interior voxels.

The ALPS index was computed for all subjects at two fixed z-levels: the standard MNI coordinate (z = 23 mm) used by Nakaya et al. (2025) and a second coordinate (z = 28 mm). The ROIs were positioned at z = 23 mm in MNI152 space such that the centrum semiovale, (projection fibres and association fibres) and the perivascular spaces are anatomically well separated. The z = 28 mm coordinate was selected after inspecting a few representative subjects to confirm adequate visualization of the projection and association fiber ROIs and the absence of the lateral ventricle at that level. The two z-levels were compared to assess how slice selection affects the ALPS index and assess whether the standard z = 23 mm coordinate was suitable for the cohort. Nakaya et al. (2025) compared the ALPS index across amyloid-stratified groups, with HC and SCD further divided into Aβ-negative and Aβ-positive groups, along with MCI and AD. In this study, we examine longitudinal changes in the ALPS index across diagnostic transitions in CN, MCI, and AD. SCD was not included in the ADNI-derived cohort.

Based on changes in diagnosis over time, subjects were classified as stable (Stable CN, Stable MCI, Stable AD), progressive (CN to MCI, MCI to AD, CN to AD), or showing diagnostic

reversal (MCI to CN, AD to MCI). The analysis examines glymphatic changes across stable, progressive, and reversed diagnostic trajectories rather than cross-sectional differences between diagnostic groups.

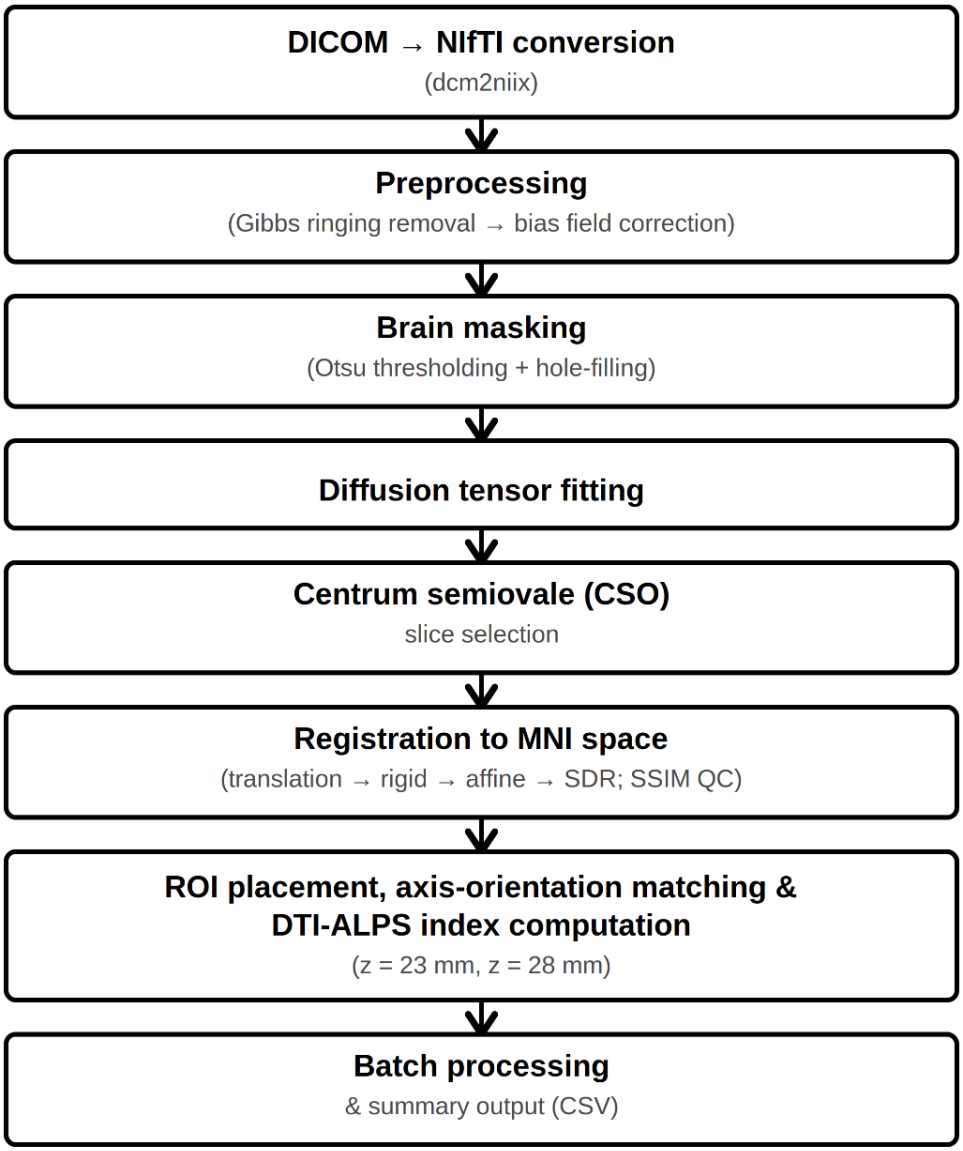


Figure 2.1. Overview of the DTI-ALPS processing pipeline. Each stage, from DICOM-to-NIfTI conversion through preprocessing, tensor fitting, registration, ROI placement, and index computation, is shown in the order applied to every subject in the final pipeline.

2.1 Dataset

The dataset used in this study was obtained from the Alzheimer's Disease Neuroimaging Initiative (ADNI) data repository (https://adni.loni.usc.edu). ADNI has four major protocol phases: ADNI 1, ADNI 2, ADNI 3, and ADNI 4. Of these four phases, DTI scans are available only for ADNI 2, ADNI 3, and ADNI 4. The DTI pipeline was applied to 201 subjects with two or more DTI scans, yielding a total of 793 scans. After pipeline processing, 12 subjects were excluded because artifacts within the ROI left fewer than two scans suitable for longitudinal comparison, leaving 189 subjects for further evaluation. The remaining subjects were screened for the following exclusion criteria: (1) a fluctuating (non-monotonic) diagnostic trajectory, (2) statistical outlier status, (3) a reversal from Alzheimer's disease (AD) to cognitively normal (CN), as this transition is not consistent with the natural progression of Alzheimer's disease, and (4) additional subjects excluded following manual review for data quality, including unusually high ALPS index values and incomplete scan-level data. These exclusions resulted in a final cohort of 173 subjects. Baseline and last available diagnoses were obtained from the diagnostic summary table 'DXSUM' from the ADNI portal. MMSE was selected as the cognitive measure because it was available for the majority of subjects across the three ADNI protocol phases included in this study. MMSE scores were used solely as numerical study variables, as recorded in the ADNI database. No MMSE test items, questions, or instrument content are reproduced in this article. The MMSE is a copyrighted instrument and may not be used or reproduced in whole or in part, in any form or language, or by any means without the written permission of PAR (www.parinc.com). Permission from Psychological Assessment Resources, Inc. (PAR) for the use of MMSE data in this publication has been obtained.

2.2 Data Conversion

The overall DTI-ALPS processing pipeline is summarised in Figure 2.1. The DTI data obtained from ADNI were provided in DICOM format. The DICOM images were converted to NIfTI format using dcm2niix because the subsequent neuroimaging tools, including DIPY, operate on volumetric NIfTI images rather than individual DICOM slices. During conversion, `dcm2niix` reconstructed the individual DICOM slices into a single 4D NIfTI volume. It also extracted the diffusion gradient directions to generate the .bvec file and the corresponding diffusion weighting values(b-values) to generate the .bval file. Spatial location and orientation information were retained from the scanner metadata. The NIfTI header confirmed that the original spatial orientation and dimensions were retained. The image orientation after conversion was verified from the NIfTI header and confirmed to be Left-Anterior-Superior(LAS).

2.3 Data Preprocessing

The DTI data were pre-processed after DICOM-to-NIfTI conversion. Preprocessing included Gibbs ringing artifact removal followed by bias field correction. The MP-PCA denoising step used by Taoka et al. (2017, 2022) and Nakaya et al. (2025) was evaluated in a pilot comparison. MP-PCA denoising produced voxel dropout (‘black spots’) within the ROI in 10 of 23 scans (43.5%), compared with 1 of 23 scans (4.3%) without denoising. Based on this comparison, MP-PCA denoising was not included in the final pipeline. Gibbs ringing artifact removal was

performed using the `gibbs_removal()` function from the `dipy.denoise.gibbs` module, which implements the local sub-voxel shift method described by Kellner et al. (2016).

Bias-field inhomogeneity can affect signal intensity across the image. Nakaya et al. (2025) included bias-field correction in their `MRtrix3-based` preprocessing pipeline. A Gaussian filter with a standard deviation (σ) of 20 voxels was applied to the mean image obtained by averaging all diffusion volumes with b-values less than 50 s/mm² to estimate the slowly varying bias field. Voxels with zero or negative values in the estimated bias field were assigned a value of one to prevent division by zero during intensity scaling. A voxel-wise scaling factor was calculated as the ratio of the global mean intensity of this image to the estimated bias field. The resulting scaling factor was applied to all diffusion volumes using NumPy broadcasting to generate the bias-corrected diffusion dataset.

2.4 Brain Masking & Tensor Fitting

A brain mask was generated from a mean b = 0 image, obtained by averaging all diffusion volumes with b-values less than 50 s/mm², using the `median_otsu()` function. The function applies a median filter with a radius of two voxels for one pass `(numpass = 1)` to smooth the image, followed by Otsu thresholding to separate brain tissue from the background and generate the initial brain mask.

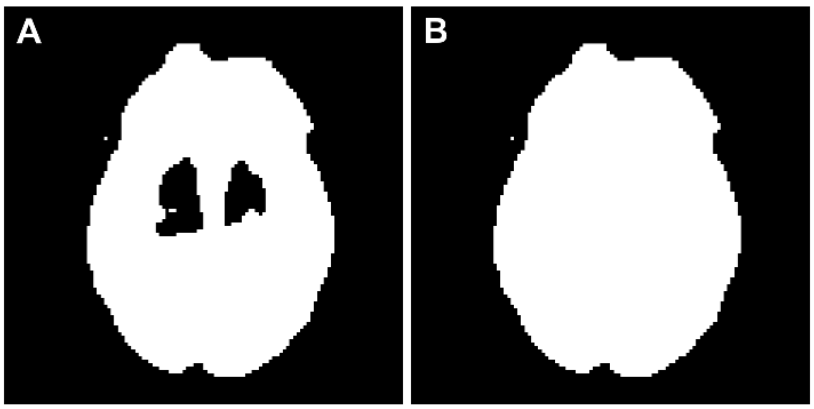


Figure 2.2. Brain mask correction via slice-wise hole-filling. Panel A: initial brain mask generated by Otsu thresholding, showing an enclosed interior hole in a superior axial slice near the centrum semiovale. Panel B: the same mask after slice-wise hole-filling, with the interior hole restored and the outer mask boundary unchanged.

Visual inspection of the initial brain mask showed enclosed holes in the superior axial slices of some subjects as shown in Figure 2.2A. These holes appeared as dark regions in the corresponding fractional anisotropy (FA) maps near the centrum semiovale, where the DTI-ALPS ROIs are located. To correct this, the binary_fill_holes() function from the `scipy.ndimage` module (Virtanen et al., 2020) was applied independently to each axial slice of the brain mask. This operation filled enclosed holes without altering the outer boundary of the brain mask (Figure 2.2B). The corrected brain mask was used for diffusion tensor fitting.

Diffusion tensor fitting was performed using the `TensorModel` class from the `dipy.reconst.dti` module (Garyfallidis et al., 2014). The diffusion gradient directions and

corresponding b-values were combined into a GradientTable object using the `gradient_table()` function. The resulting GradientTable was used to fit the tensor model to the preprocessed diffusion data within the corrected brain mask.

The diffusion tensor model is based on the Stejskal-Tanner equation (Stejskal & Tanner, 1965) and the tensor formulation (Basser et al., 1994) :

$$S = S_0 \exp(-b\, g^T D\, g) \quad \textit{Eq (1)}$$

where S is the diffusion-weighted signal, S_0 is the non-diffusion-weighted (b = 0) signal, b is the diffusion weighting factor, g is the unit gradient direction vector, and D is the 3 × 3 diffusion tensor.

The fitted tensor was used to derive the fractional anisotropy (FA) map, the primary eigenvectors, and the diagonal tensor elements (D_{xx}, D_{yy}, and D_{zz}), representing diffusivity along the image x-, y-, and z-axes, respectively. Negative values of D_{xx}, D_{yy}, and D_{zz} were set to zero using the `np.clip()` function. Mean FA and MD were used as quality-control measures for the tensor fit.

2.5 Centrum Semiovale Slice Selection

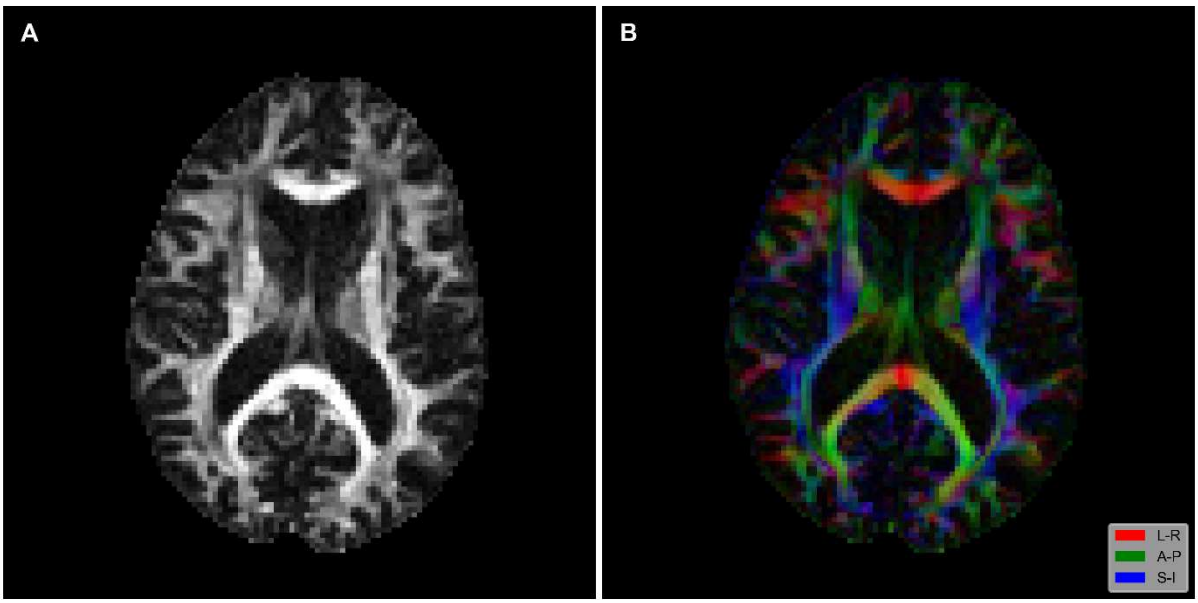


Figure 2.3. Directionally encoded colour (DEC) fractional anisotropy map at the centrum semiovale slice used for DTI-ALPS ROI placement. Panel A: fractional anisotropy (FA) map of the slice in greyscale. Panel B: the same slice as a DEC-FA map, where voxel colour reflects the primary eigenvector direction weighted by FA: red indicates fibres running left-right, the orientation of the perivascular space; green indicates association fibres (anterior-posterior); and blue indicates projection fibres (superior-inferior). The expected pattern, a red projection tract flanked by green association regions, confirms correct slice selection.

The DTI-ALPS index is calculated from ROIs positioned in the centrum semiovale, a region of dense white matter superior to the lateral ventricles (Taoka et al., 2017). The centrum

semiovale slice must therefore be selected carefully for DTI-ALPS index calculation. After tensor fitting, an FA slice grid was created showing all axial slices of the native-space volume. The centrum semiovale was identified on the axial slices of the MRI as the highest slice with a continuous ring of bright white matter, without the dark "butterfly"-shaped cavity of the lateral ventricles. This slice was manually recorded as CENTRUM_SEMIOVALE_SLICE. The manually selected native-space slice was then compared with the standard MNI coordinate used for ROI placement. In this map, projection fibres appear blue (superior-inferior), association fibres appear green (anterior-posterior), and subcortical fibres running in the left-right direction, the orientation along which the perivascular space itself runs, appear red as seen in figure 2.3. A lateral blue projection fibre tract flanked by green association fibre regions was expected at the proper centrum semiovale level, indicating anatomical appropriateness of the slice at which the ALPS ROIs were placed.

2.6 Registration to MNI Standard Space

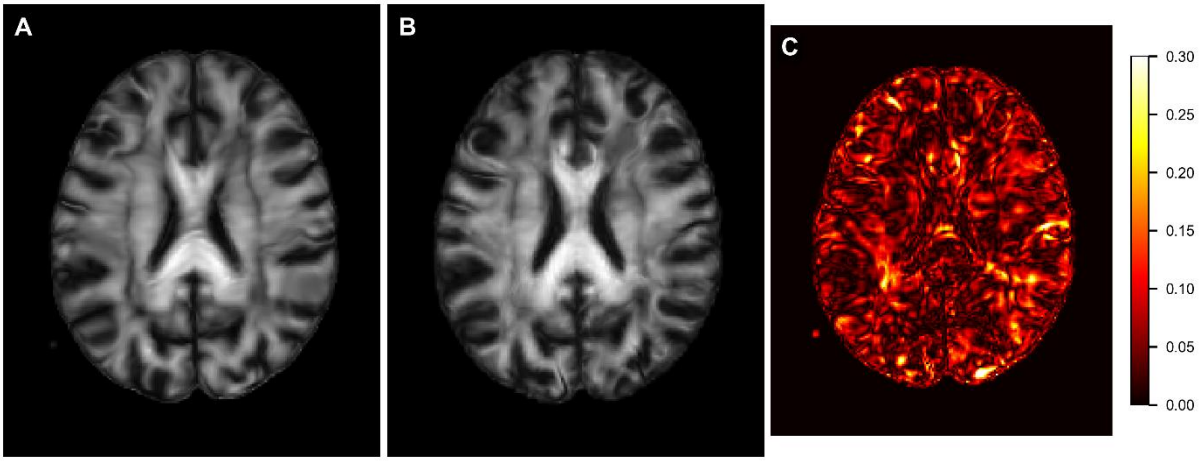


Figure 2.4: Registration quality control for a representative subject. Panel A: the FMRIB58_FA_1mm template. Panel B: the subject's FA map after four-stage registration (translation, rigid, affine, symmetric diffeomorphic registration) to the template. Panel C: the voxel-wise absolute difference between the registered subject FA map and the template, with the colour scale indicating the magnitude of residual misalignment.

Registration to a common standard space allows the same MNI coordinates to be used for ROI placement across subjects, despite differences in brain size, shape, and scanner positioning. Figure 2.4 shows the FMRIB58_FA_1mm template provided by FSL and created by averaging the FA maps of 58 healthy subjects in MNI space at an isotropic resolution of 1 mm. Both Nakaya et al. (2025) and Taoka et al. (2017, 2022) used linear (FSL FLIRT) and nonlinear (FSL FNIRT) registration. Because FSL is Linux-based, registration in the present study was performed using `dipy.align`, a pure-Python implementation suitable for Windows (Garyfallidis et al., 2014). Registration was carried out in four sequential stages, each initialized from the result of the preceding stage. The four stages were translation (3 degrees of freedom) to correct scanner-position offsets; rigid registration (6 degrees of freedom) to correct head tilt and rotation; full affine registration (12 degrees of freedom) to account for differences in brain size through scaling and shearing; and symmetric diffeomorphic registration (SDR) to achieve nonlinear alignment of anatomical features such as ventricle shape, sulcal patterns, and white

matter tract geometry. Full parameter values for each registration stage are provided in Supplementary Table S3.

2.7 Axis Orientation Check

The DTI-ALPS index depends on a particular diagonal element of the diffusion tensor because the numerator of the formula requires diffusivity along the left-right anatomical direction. The array axis corresponding to the left-right direction is not fixed and is determined by the affine matrix of the image. Native subject scans do not necessarily share the same axis convention as the template. The perivascular axis was identified from the template affine only, after the subject's diffusivity maps (D_{xx}, D_{yy}, D_{zz}) were resampled into template space using `mapping.transform()`. Once resampled, these maps follow the template's axis ordering, independent of the native scan's original orientation. Based on the template's axis codes, the array axis corresponding to left-right was identified programmatically, and the diffusivity value at that axis was used as the numerator in the ALPS formula. The anterior-posterior diffusivity was used as the denominator for the projection-fiber ROIs, and the superior-inferior diffusivity was used as the denominator for the association-fiber ROIs. This follows the ALPS formulation reported by Taoka et al. (2017, 2022).

A worked example for a representative subject is provided in Supplementary Table S4. The assigned axis determines the diffusivity component used for the perivascular-space direction, even if the left-right axis occupies a different array position. The check identifies only the left-right axis. The remaining two axes are assumed to follow standard NIfTI ordering rather than being independently verified, and the pipeline has not been tested on templates where this assumption fails. The same FMRIB58 template object was loaded once and used for registration across all subjects in the batch pipeline, so the template's axis codes and the resulting axis assignment were identical for every subject processed.

2.8 ROI Placement and ALPS Index Computation

2.8.1 ROI Coordinates

Four spherical ROIs were located in MNI space at the coordinates shown in (Supplementary Table S1), corresponding to the projection and association fiber areas bilaterally. The coordinates were selected based on their established use in the DTI-ALPS literature and were not independently re-derived in this study.

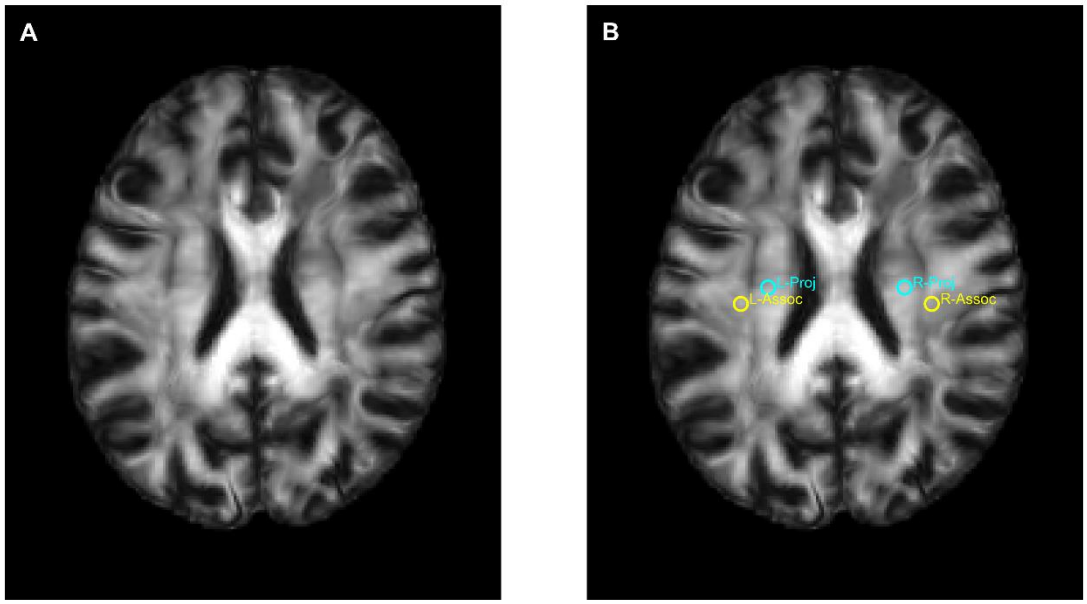


Figure 2.5. Placement of the four DTI-ALPS regions of interest at the standard MNI z = 23 mm level, shown on the FMRIB58 template. Panel A: the unlabeled template slice. Panel B: the same slice with the four regions of interest marked and labelled, left and right projection fibre ROIs (L-Proj, R-Proj) and left and right association fibre ROIs (L-Assoc, R-Assoc), corresponding to the coordinates listed in Table 2.1.

In MNI space, z = 23 mm was used as the standard centrum semiovale level (Figure 2.5). The ALPS index was also calculated at a z-coordinate manually selected based on the subject-specific centrum semiovale slice identified in native space, to assess the effect of ROI z-level on the ALPS index. Each ROI was created as a sphere of radius 2.5 mm centered at the converted voxel coordinates, resulting in approximately 81 voxels per ROI at 1 mm isotropic resolution. Mean diffusivity for each sphere was calculated excluding voxels with zero values, corresponding to background or registration gaps.

2.8.2 ALPS Computation

The ALPS index was calculated bilaterally using the formula devised by Taoka et al. (2017):

$$ALPS = \text{mean}(D_{xx},\text{proj}, D_{xx},\text{assoc}) / \text{mean}(D_{yy},\text{proj}, D_{zz},\text{assoc}) \quad \textit{Eq.(2)}$$

D_{xx},proj and D_{xx},assoc are the mean left-right diffusivity values in the projection fiber ROI and association fiber ROI, respectively; D_{yy},proj is the mean anterior-posterior diffusivity in the projection fiber ROI; and D_{zz},assoc is the mean superior-inferior diffusivity in the association fiber ROI. ALPS values were calculated separately for the left and right hemispheres and then averaged to obtain the final bilateral ALPS index. Higher ALPS values indicate greater relative diffusivity along the perivascular direction and are generally interpreted as reflecting better glymphatic function. Lower ALPS values have been associated with reduced glymphatic function and cognitive decline across CN, MCI, and AD diagnostic groups (Bao et al., 2025; Nakaya et al., 2025; Taoka et al., 2017). The pipeline was implemented in Python using DIPY, NumPy, and SciPy (see Supplementary Material Table S5). Processing required approximately 45 minutes per subject. A complete list of the libraries and functions used at each processing step, together with runtime and implementation details, is provided in Supplementary Table S6.

2.9 Statistical Analysis

Baseline absolute ALPS index values across the CN, MCI, and AD diagnostic groups were compared using both the Kruskal-Wallis test and one-way ANOVA. Epsilon-squared and eta-squared effect sizes were reported for the Kruskal-Wallis test and ANOVA, respectively. Longitudinal change scores (%ALPS change, annualized %ALPS change, and %MMSE change) between the Stable MCI and MCI-to-AD subgroups were first assessed using Levene's test for variance homogeneity. Welch's t-test (unequal variance) and the Mann-Whitney U test were then applied in parallel, with Cohen's d and its 95% confidence interval reported as standardized effect sizes.

The association between %ALPS change and %MMSE change was assessed using both Pearson's r and Spearman's ρ, each reported with a 95% confidence interval, R^2, and p-value. Group overlap between adjacent diagnostic and trajectory groups was quantified as the percentage of one group's values falling within the full range of the comparison group and, separately, within its IQR. The same metric was applied to the absolute baseline ALPS index and to the %ALPS and %MMSE change scores, allowing overlap to be compared directly.

Single-predictor discrimination of conversion status (Stable MCI vs. MCI-to-AD) was evaluated using receiver operating characteristic (ROC) analysis. The optimal cut point was selected by maximizing Youden's index, and 95% confidence intervals for AUC were obtained using bootstrap resampling. A logistic regression model combining %ALPS change and %MMSE change as standardized predictors was fit to assess their combined discrimination and independent contributions, with standardized coefficients, standard errors, z-statistics, p-values, and odds ratios (95% CI) reported for each term. Combined-model discrimination was evaluated using leave-one-out cross-validation (LOOCV), and AUC differences between the combined and single-predictor models were tested via paired bootstrap resampling. For robustness, the combined model was refit after iteratively removing the most extreme subjects. AUC was recomputed after each removal to determine whether individual cases influenced the classification result.

3. Results

3.1 Pipeline Validation and Denoising Comparison

MP-PCA denoising was evaluated using a representative subset of 23 DTI scans. With the denoising step included, the ALPS index could be computed for 13 of the 23 scans at both the z = 23 mm and z = 28 mm coordinates. For the remaining 10 scans, ALPS computation could not be performed because black spot artifacts were present within the region of interest (ROI). When the denoising step was removed, the yield increased substantially. A valid index was obtained for 22 of 23 scans (95.7%) at z = 23 mm and for all 23 scans (100%) at z = 28 mm. Only one scan (subject 021_S_4254, image I273272) continued to show black-spot artifacts within the ROI at the z = 23 mm coordinate after denoising was removed.(See supplementary material, Table S2)

For scans in which the ALPS index could be computed using both processing pipelines, the computed ALPS differed only slightly between the denoised and non-denoised datasets.

Removal of the denoising step also reduced the occurrence of black spot artifacts within the ROI, allowing ALPS indices to be computed for more scans. Based on these observations, MP-PCA denoising was excluded from the final processing pipeline used for all subsequent analyses.

3.2 Baseline (absolute) ALPS overlap across diagnostic groups

Before examining longitudinal changes, the absolute ALPS index at baseline was characterized according to each subject's baseline diagnosis: Cognitively Normal (CN), Mild Cognitive Impairment (MCI), or Alzheimer's Disease (AD). Trajectory-defined subgroups, such as MCI-to-AD converters, CN-to-AD converters, CN-to-MCI converters, and diagnostic reversals, were not used at this stage. These categories depend on the subject's subsequent clinical course and, therefore, were not known at baseline. The baseline analysis was consequently restricted to CN, MCI, and AD.

Table 3.1. Descriptive statistics for the absolute single-timepoint DTI-ALPS index at baseline, by diagnostic group (CN, MCI, AD).

Group	N	Mean	SD	Median	Q1	Q3	Min	Max
CN	68	1.327	0.199	1.361	1.205	1.457	0.73	1.729
MCI	92	1.336	0.195	1.335	1.213	1.451	0.946	2.004
AD	13	1.094	0.169	1.1	0.989	1.251	0.797	1.379

Table 3.1 shows that the AD group (N = 13) was substantially smaller than the CN (N = 68) and MCI (N = 92) groups. Estimates involving the AD group, particularly comparisons between AD and the other diagnostic groups, should therefore be interpreted cautiously given the smaller sample size. The CN (n = 68) and MCI (n = 92) groups showed similar central tendencies, with mean ALPS indices of 1.327 and 1.336 and median values of 1.361 and 1.335, respectively. The AD group (n = 13) showed lower mean and median ALPS indices of 1.094 and 1.100, respectively. However, these group-level differences do not indicate whether ALPS values can distinguish individual subjects across diagnostic groups. Baseline MMSE was not available for as many subjects as baseline ALPS index (CN: n=61 vs. n=68; MCI: n=74 vs. n=92; AD: n=13 for both), reflecting incomplete baseline neuropsychological data for some subjects with a computable baseline ALPS value.

The same methodology was used to quantify group overlap at baseline and in the longitudinal change scores. Group overlap was defined as the percentage of individual values from one group that fell within the full range and, separately, within the interquartile range (IQR) of an adjacent group. Using the same definition allows overlap values from the baseline and longitudinal analyses to be compared directly.

At baseline, absolute DTI-ALPS index values overlapped substantially between adjacent diagnostic groups. Between CN and MCI, 95.6% of CN subjects' values fell within the full range of MCI values, and 96.7% of MCI subjects' values fell within the full range of CN values; restricting the comparison to the interquartile range, 45.6% of CN values fell within the MCI

IQR, and 52.2% of MCI values fell within the CN IQR. Between MCI and AD, full-range overlap remained substantial (62.0% of MCI values fell within the AD range; 84.6% of AD values fell within the MCI range), while IQR-based overlap was lower and more symmetric (30.4% of MCI values fell within the AD IQR; 30.8% of AD values fell within the MCI IQR). Baseline MMSE scores showed a similar pattern of overlap between adjacent diagnostic groups, with greater overlap between CN and MCI than between MCI and AD (Table 3.2).

Table 3.2. Overlap in absolute baseline MMSE score between adjacent diagnostic groups (CN vs. MCI, MCI vs. AD), using the same range and interquartile-range overlap metric applied to baseline DTI-ALPS index.

Comparison	Group	% Within Adjacent Range	% Within Adjacent IQR
CN vs MCI	CN	100	52.5
CN vs MCI	MCI	100	52.7
MCI vs AD	MCI	47.3	2.7
MCI vs AD	AD	53.8	7.7

To assess whether the baseline values differed across diagnostic categories, both the Kruskal-Wallis test and one-way ANOVA were applied to baseline ALPS and baseline MMSE (Table 3.3). Both tests indicated a statistically significant difference among the baseline ALPS values of the CN, MCI, and AD groups (Kruskal-Wallis $H = 15.15$, $p = 0.000513$; one-way ANOVA $F = 8.991$, $p = 0.000194$).

Table 3.3. Kruskal-Wallis and one-way ANOVA comparison of absolute baseline DTI-ALPS index and MMSE score across CN, MCI, and AD, with epsilon-squared and eta-squared effect sizes.

Variable	Test	Statistic	p	Effect Size Measure	Effect Size	Effect Size Label
Absolute Baseline DTI-ALPS Index	Kruskal-Wallis	15.15	0.0005	epsilon-squared	0.088	medium
Absolute Baseline DTI-ALPS Index	One-way ANOVA	8.991	0.0002	eta-squared	0.096	medium
Absolute Baseline MMSE Score	Kruskal-Wallis	43.9	<0.001	epsilon-squared	0.299	large
Absolute Baseline MMSE Score	One-way ANOVA	76.563	<0.001	eta-squared	0.514	large

The baseline ALPS index values differed significantly among the diagnostic groups, while substantial overlap remained between individual subjects across all three groups. Figure 3.1 shows the absolute baseline ALPS index as a boxplot with individual subject values overlaid, illustrating the extent of overlap between diagnostic groups. Similarly, Figure 3.2 shows the corresponding boxplot of baseline MMSE scores by diagnostic group.

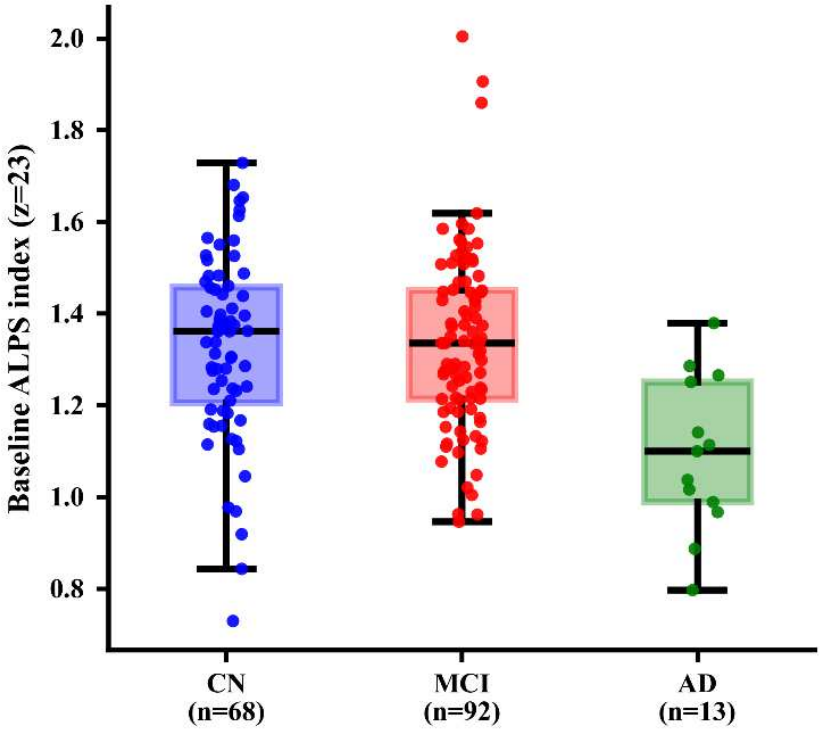


Figure 3.1. Distribution of absolute baseline DTI-ALPS index by diagnostic group (CN, MCI, AD). Boxes show the median and interquartile range; individual subject values are overlaid to show the extent of overlap between groups.

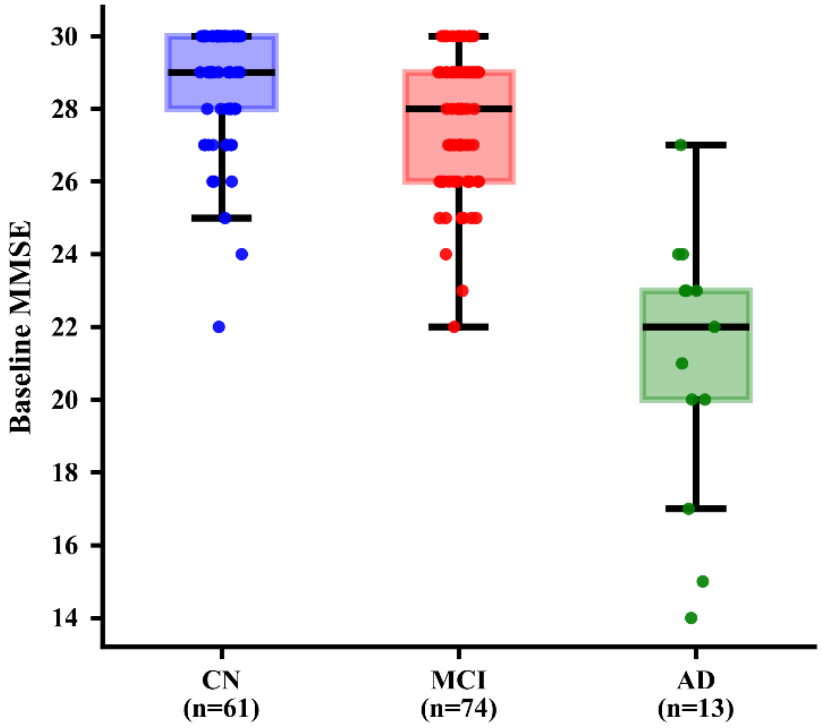


Figure 3.2. Distribution of absolute baseline MMSE score by diagnostic group (CN, MCI, AD). Boxes show the median and interquartile range; individual subject values are overlaid to show the extent of overlap between groups.

3.3 Sample accounting

The available sample sizes for the Stable MCI and MCI-to-AD converter subgroups are reported first because they determine the sample sizes used in the subsequent analyses. Among the subjects eligible for the Stable MCI versus MCI-to-AD comparison, 68 had a computable %ALPS change value, 52 had a computable %MMSE change value, and 52 had both measures available. The lower availability of %MMSE change compared with %ALPS change reflects incomplete longitudinal cognitive test follow-up in a subset of subjects for whom imaging follow-up was available. Accordingly, analyses from Section 3.7 onward that directly compare or jointly model %ALPS change and %MMSE change are restricted to this common subsample of n = 52. Analyses of %ALPS change alone in Sections 3.4-3.6 and 3.8 use the full sample of N = 68 where applicable.

3.4 Descriptive statistics for %ALPS change and %MMSE change

Longitudinal percentage changes in the ALPS index and MMSE score from baseline to follow-up were compared between subjects classified as Stable MCI (n = 36 for %ALPS change; n = 30 for %MMSE change) and those who converted from MCI to AD (n = 32 for %ALPS change; n = 22 for %MMSE change) during the available follow-up period. Full descriptive statistics for both variables and groups are presented in Table 3.4.

Table 3.4. Descriptive statistics for percentage change from baseline in DTI-ALPS index and MMSE score, comparing Stable MCI and MCI-to-AD subjects.

Variable	Group	N	Mean (SD) [95% CI]	Median [Q1, Q3]	Range [Min, Max]
% ALPS Change	Stable MCI	36	-0.45 (6.40) [-2.66, 1.67]	-0.41 [-4.68, 3.5]	[-15, 14.92]
% ALPS Change	MCI to AD	32	-5.64 (10.09) [-9.27, -2]	-5.5 [-14.20, 1.832]	[-22.3, 13.7]
MMSE % Change	Stable MCI	30	-2.87 (7.39) [-5.63, -0.11]	0 [-3.45, 0]	[-21.43, 7.692]
MMSE % Change	MCI to AD	22	-16.26 (11.84) [-21.51, -11.01]	-16.33 [-25.40, -10]	[-38.46, 3.704]

On average, the MCI-to-AD group showed greater decline than the Stable MCI group on both measures. The mean decline in ALPS index was approximately 5.1 percentage points greater in the MCI-to-AD group (-5.637% vs. -0.5%), while the mean decline in MMSE score was approximately 13.4 percentage points greater (-16.259% vs. -2.868%). The Stable MCI group had a median %MMSE change of 0.000, indicating that at least half of the subjects in this group showed no net change in MMSE score over the follow-up period. In contrast, the MCI-to-AD group had a median %MMSE change of -16.333%, indicating a substantial decline in MMSE

score. Figure 3.3 shows paired boxplots of %ALPS change and %MMSE change for the two groups, with individual subject values overlaid.

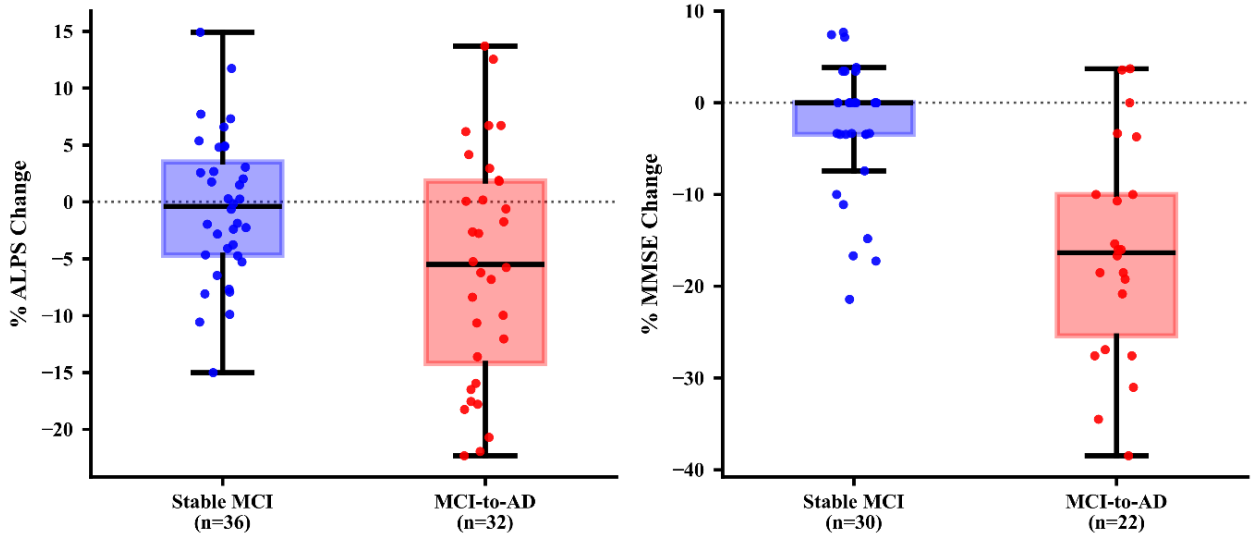


Figure 3.3. Percentage change from baseline, by group (Stable MCI vs. MCI-to-AD). Panel A: DTI-ALPS index. Panel B: MMSE score. Boxes show the median and interquartile range; individual subject values are overlaid

3.5 Overlap quantification for change scores

For comparison with the baseline overlap analysis in Section 3.2, the proportion of Stable MCI subjects whose decline was at least as large as the median decline observed in the MCI-to-AD group was calculated separately for %ALPS change and %MMSE change (Table 3.5).

Table 3.5. Percentage of Stable MCI subjects whose percentage change from baseline, in DTI-ALPS index and MMSE score, respectively, was at least as large in magnitude as the median decline observed in the MCI-to-AD group.

Variable	MCI-to-AD Median	N (Stable MCI)	% Stable MCI as Extreme
% ALPS Change	-5.5	36	19.4
MMSE % Change	-16.333	30	10

Only 19.4% of Stable MCI subjects showed a %ALPS decline at least as large as the median decline in the MCI-to-AD group, while 10.0% showed a %MMSE decline at least as large as the corresponding MCI-to-AD median. Both proportions were lower than the baseline overlap fractions reported in Section 3.2, where overlap between adjacent diagnostic groups ranged from 62% to 97%, depending on the comparison and metric.

Sections 3.2 and 3.5 compare absolute baseline values with longitudinal change. Substantial overlap was observed between diagnostic groups when the absolute, single-timepoint ALPS index was considered, whereas the overlap was lower when decline was measured relative to each subject's baseline. These findings suggest that within-subject longitudinal change

provides information that is less apparent from a single cross-sectional ALPS measurement when comparing Stable MCI with MCI-to-AD converters.

3.6 Group comparison for significance testing

Statistical comparisons of %ALPS change and %MMSE change between the Stable MCI and MCI-to-AD groups were performed using both parametric and non-parametric approaches because the data showed non-normal distributions and unequal variances. For each variable, Table 3.6 reports the mean difference between groups with its 95% confidence interval, Welch's t-test (unequal-variance t-test), Levene's test for homogeneity of variance, Mann-Whitney U test, and Cohen's d with its 95% confidence interval and plain-language effect-size label. Levene's test was used to assess variance homogeneity and support the use of Welch's t-test rather than Student's t-test.

Comparison of subjects with missing baseline or follow-up MMSE data (n = 16) against complete cases (n = 52), across the three primary outcome variables, can be seen in S7(Supplementary material). For each variable, the median value among subjects with missing MMSE is compared to the median among complete cases using the Mann-Whitney U test to assess whether subjects with missing MMSE data differ systematically from those with complete data. None of the three comparisons reached significance (all $p > 0.05$), indicating no evidence that MMSE missingness was associated with %ALPS change, annualized %ALPS change, or years of follow-up, consistent with data missing at random with respect to these variables rather than a systematic pattern of missingness.

Table 3.6. Statistical comparison of %ALPS change and %MMSE change between Stable MCI and MCI-to-AD subjects, including the mean difference with 95% confidence interval, Welch's t-test, Levene's test for variance homogeneity, the Mann-Whitney U test, and Cohen's d with 95% confidence interval and effect-size label. Values in brackets indicate 95% confidence intervals, except where noted as p-values; the t-statistic, U-statistic, and Levene's statistic are each followed by their corresponding p-value in brackets.

Variable	Mean Diff [95% CI]	Welch's t [p]	Levene's Stat [p]	Mann-Whitney U [p]	Cohen's d [95% CI], label
% ALPS Change	5.142 [0.971, 9.312]	2.475 [0.0167]	8.691 [0.0044]	753 [0.0301]	0.617 [0.129, 1.104], medium
MMSE % Change	13.392 [7.567, 19.216]	4.679 [<0.001]	4.61 [0.0367]	538.5 [0.0001]	1.407 [0.794, 2.021], large

For both variables, Levene's test indicated unequal variances between the groups ($p = 0.0044$ for %ALPS change; $p = 0.0367$ for %MMSE change), supporting the use of Welch's t-test rather than the standard Student's t-test, which assumes equal variances. Both %ALPS change and %MMSE change differed significantly between the Stable MCI and MCI-to-AD groups in both the parametric (Welch's t-test) and non-parametric (Mann-Whitney U) analyses.

For %ALPS change, the mean difference was 5.142 percentage points (95% CI: 0.971–9.312; Welch's t = 2.475, p = 0.0167; Mann-Whitney U = 753, p = 0.0301), corresponding to a medium effect size (Cohen's d = 0.617, 95% CI: 0.129–1.104). For %MMSE change, the mean difference was 13.392 percentage points (95% CI: 7.567–19.216; Welch's t = 4.679, p < 0.001; Mann-Whitney U = 538.5, p = 0.0001), corresponding to a large effect size (Cohen's d = 1.407, 95% CI: 0.794-2.021).

3.7 Correlation between %ALPS change and %MMSE change

The association between %ALPS change and %MMSE change was assessed among the n = 52 subjects with both measures available (Section 3.3), using both Pearson's r (linear association) and Spearman's rho (monotonic, rank-based association), each with a 95% confidence interval, the coefficient of determination (R^2), and a significance test (Table 3.7).

Table 3.7. Pearson and Spearman correlation between %ALPS change and %MMSE change among the 52 subjects with both measures available, with 95% confidence intervals, coefficient of determination (R^2), and significance tests.

Method	N	r	95% CI Low	95% CI High	R^2 (%)	p
Pearson	52	0.204	-0.073	0.452	4.2	0.1463
Spearman	52	0.144	-0.134	0.401	2.1	0.3089

Both correlation coefficients were weak in magnitude and neither reached statistical significance (Pearson r = 0.204, 95% CI: -0.073 to 0.452, R^2 = 4.2%, p = 0.1463; Spearman ρ = 0.144, 95% CI: -0.134 to 0.401, R^2 = 2.1%, p = 0.3089). Given the weak correlation between the two measures, %ALPS change and %MMSE change were evaluated jointly in the logistic regression model described in Section 3.9. Figure 3.4 shows the relationship between %ALPS change and %MMSE change as a scatter plot, with individual subjects colored by diagnostic trajectory group. The fitted regression line and 95% confidence band illustrate the weak association and substantial scatter between the two measures, consistent with the correlation results reported in Table 3.7.

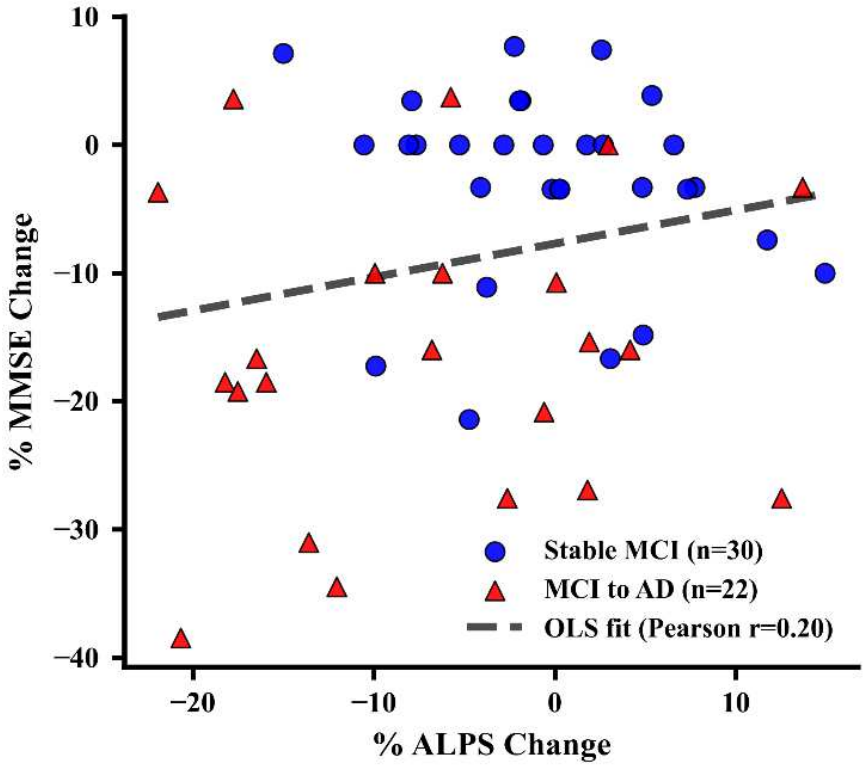


Figure 3.4. Relationship between %ALPS change and %MMSE change (n = 52), one point per subject, coloured by diagnostic trajectory group (Stable MCI, MCI-to-AD). The dashed line shows the fitted ordinary least squares regression (Pearson r = 0.20), illustrating the weak, non-significant association reported in Table 3.7.

3.8 Single Predictor Discrimination: ROC/AUC Analysis

The ability of each change score to discriminate MCI-to-AD converters from Stable MCI subjects was evaluated using receiver operating characteristic (ROC) analysis. For each predictor, Table 3.8 reports the area under the curve (AUC), the optimal cut point (identified by maximizing Youden's index), sensitivity, specificity, positive predictive value (PPV), negative predictive value (NPV), overall accuracy, and the confusion-matrix counts.

Table 3.8. Classification performance of %ALPS change and %MMSE change, evaluated separately, for distinguishing MCI-to-AD converters from Stable MCI subjects.

Predictor	N	AUC	Cut point	Sensitivity	Specificity	PPV	NPV	Acc	TP	FP	FN	TN
% ALPS Change	68	0.654	-8.37	0.406	0.917	0.812	0.635	0.676	13	3	19	33
MMSE % Change	52	0.816	-3.704	0.818	0.767	0.72	0.852	0.788	18	7	4	23

%ALPS change alone achieved modest discrimination (AUC = 0.654), with high specificity (0.917) but low sensitivity (0.406) at its optimal cut point of -8.37. %MMSE change alone achieved substantially stronger discrimination (AUC = 0.816), with a more balanced sensitivity (0.818) and specificity (0.767) at its optimal cut point of -3.704%. The 95% confidence

intervals for the AUC estimates were obtained using bootstrap resampling for each predictor (Supplementary material Table S8). The 95% confidence interval for %ALPS change (0.514-0.783) includes the 0.5 no-discrimination threshold, whereas the interval for %MMSE change (0.681-0.930) lies entirely above it. This is consistent with %MMSE change showing stronger single-predictor discrimination. Figure 3.5 shows the ROC curves for the two predictors with their AUC values, allowing direct comparison of their discriminative performance across the range of cut points.

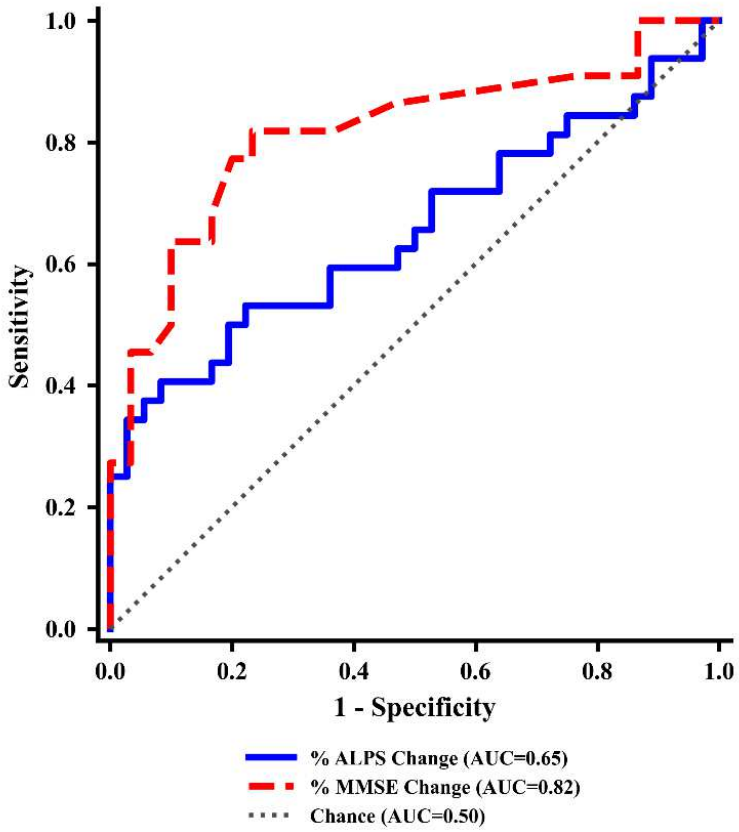


Figure 3.5. Receiver operating characteristic (ROC) curves for %ALPS change and %MMSE change as single predictors of MCI-to-AD conversion, with AUC values labeled and the chance-level diagonal (AUC = 0.50) shown for reference.

3.9. Combined logistic regression model, ALPS change and MMSE change as joint predictors of conversion

Because %ALPS change and %MMSE change showed only a weak, non-significant correlation with one another (Section 3.7), a logistic regression model combining both predictors was fit to evaluate their joint discriminative performance and independent contributions to conversion status.

(a) Combined classification performance: The combined model was evaluated using leave-one-out cross-validation (LOOCV) to reduce the risk of overfitting, given the modest sample size. Results are reported alongside the two single-predictor models using the same metrics as in Section 3.8 (Table 3.9).

Table 3.9. Classification performance of the combined logistic regression model (leave-one-out cross-validation), shown alongside the two single-predictor models from Table 3.8 for direct comparison.

Predictor	N	AUC	Cut point	Sensitivity	Specificity	PPV	NPV	Acc	TP	FP	FN	TN
% ALPS Change	68	0.654	-8.37	0.406	0.917	0.812	0.635	0.676	13	3	19	33
MMSE % Change	52	0.816	-3.704	0.818	0.767	0.72	0.852	0.788	18	7	4	23
Combined (LOOCV)	52	0.809	0.41	0.818	0.833	0.783	0.862	0.827	18	5	4	25

The combined model achieved an AUC of 0.809 under LOOCV, with a sensitivity of 0.818, a specificity of 0.833, and an overall accuracy of 0.827. It had the highest accuracy among the three models, while its sensitivity matched that of %MMSE change alone, and its specificity was higher than %MMSE change alone (0.833 vs. 0.767), though lower than %ALPS change alone (0.917)."

(b) Independent contribution of each predictor: The independent contribution of each predictor was assessed using standardized logistic regression coefficients, standard errors, z-statistics, p-values, and odds ratios with 95% confidence intervals for each term in the joint model (Table 3.10).

Table 3.10. Standardized coefficients from the combined logistic regression model of %ALPS change and %MMSE change predicting conversion status, with standard errors, z-statistics, p-values, and odds ratios with 95% confidence intervals.

Term	Coef. (SE) [95% CI]	z (p)	Odds Ratio [95% CI]
Constant	-0.2884 (0.3686) [-1.0108, 0.4341]	-0.7823 (0.434)	0.7495 [0.3639, 1.5435]
% ALPS change	-0.8156 (0.4074) [-1.6142, -0.0171]	-2.0019 (0.0453)	0.4424 [0.1991, 0.9831]
% MMSE change	-1.618 (0.4688) [-2.5369, -0.6992]	-3.4515 (0.0006)	0.1983 [0.0791, 0.497]

Both standardized predictors remained statistically significant in the joint model: $ALPS_z$ (β = -0.8156, SE = 0.4074, z = -2.0019, p = 0.0453, OR = 0.4424, 95% CI: 0.1991-0.9831) and $MMSE_z$ (β = -1.6180, SE = 0.4688, z = -3.4515, p = 0.0006, OR = 0.1983, 95% CI: 0.079-0.4970).

The improvement in overall discriminative performance was assessed separately by comparing the combined model's AUC with the AUC of each single-predictor model using paired bootstrap resampling (Table S8, Supplementary material). Neither AUC difference reached statistical significance: the combined model's AUC exceeded that of %ALPS change alone by 0.117 (95% CI: -0.037 to 0.289, p = 0.14) and was essentially indistinguishable from %MMSE change alone, differing by only -0.007 (95% CI: -0.094 to 0.076, p = 0.86). These findings do not contradict the results in Table 3.10 because the two analyses address different questions. The coefficient analysis evaluates each predictor's contribution after accounting for the other predictor, whereas the AUC comparison evaluates overall discriminative performance. Thus,

the statistical significance of an individual predictor does not necessarily imply a significant improvement in overall AUC.

Figure 3.6 shows the ROC curves for %ALPS change alone, %MMSE change alone, and the combined LOOCV model, with AUC values labeled (see Table S9). The curves show the near-overlap between the %MMSE-alone and combined-model curves and the greater separation of the %ALPS-alone curve.

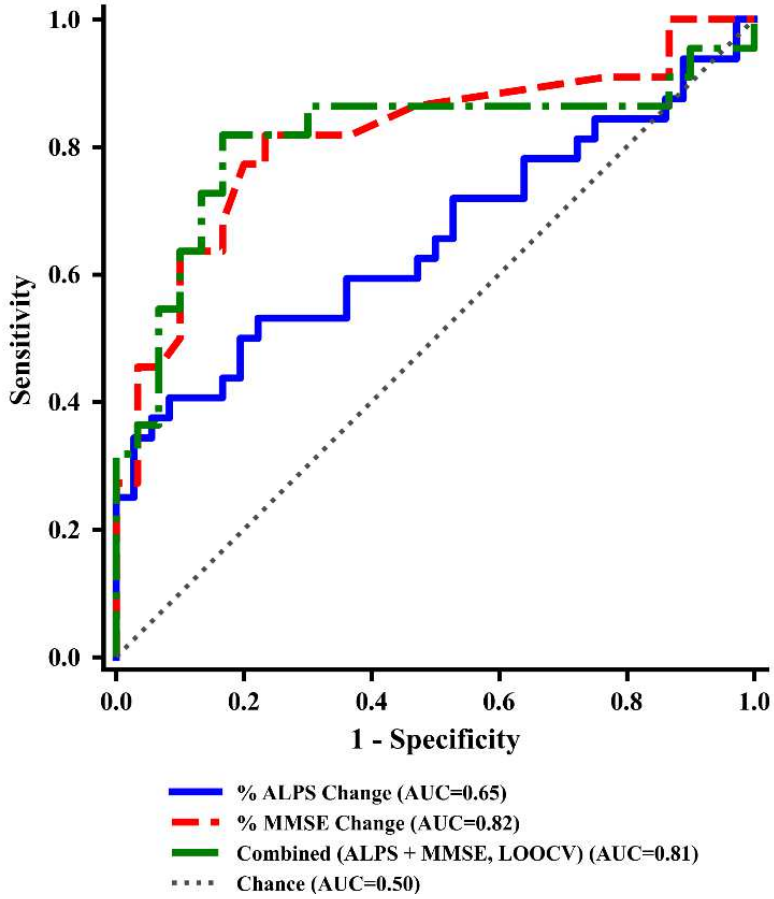


Figure 3.6. Receiver operating characteristic (ROC) curves for %ALPS change alone, %MMSE change alone, and the combined logistic regression model (leave-one-out cross-validation), with AUC values labeled and the chance-level diagonal (AUC = 0.50) shown for reference (Table S9).

3.10 Robustness check

To evaluate whether the combined model's classification performance (Section 3.9(a)) was disproportionately driven by a small number of extreme subjects, the model was refit after iteratively removing the most extreme cases and recomputing AUC (Table S10).

Removing the two most extreme subjects changed the combined model's AUC by only -0.009 (from 0.809 to 0.800), and removing the four most extreme subjects changed it by only -0.035 (to 0.774). In both cases, the resulting AUC remained within the range of the model's bootstrap confidence interval (0.662-0.935; Table S9). The AUC remained close to its original value after removing these subjects, suggesting that the joint-model result reported in Section 3.9(a) was not driven by a small number of extreme cases.

4. Discussion

Within subjects with baseline MCI, both percentage change in DTI-ALPS index and percentage change in MMSE score differed significantly between those who remained diagnostically stable and those who converted to Alzheimer's disease (Table 3.6), and both measures remained independently associated with conversion status when modelled together (Table 3.10). We evaluated the combined model's predictive performance using leave-one-out cross-validation, refitting it 52 times, each time withholding one subject and predicting their outcome from the remaining 51. Under this approach, the combined model reached an AUC of 0.809, against 0.816 for %MMSE change alone, a difference of -0.007 (95% CI: -0.094 to 0.076, p = 0.86; Table S9). That confidence interval spans zero, so the two models' discrimination is statistically indistinguishable. Adding %ALPS change did not measurably sharpen classification beyond what %MMSE change already provided. This should not be read as %ALPS change lacking biomarker value. It only means that, at this sample size, ALPS change did not outperform, or add measurably to, a simple cognitive measure for this specific task.

The clearest methodological contribution of this study is the contrast between absolute, single-timepoint ALPS values and change-from-baseline values. At baseline, ALPS overlapped substantially across CN, MCI, and AD, even though the overall group difference was statistically significant (Table 3.3). Percentage ALPS change, by contrast, separated Stable MCI from MCI-to-AD with a medium effect size (Table 3.6). Together, these results support the premise this study set out to test: change in ALPS over time carries more diagnostic information than a single measurement does. A cross-sectional ALPS reading is a weak discriminator of diagnostic status; the same measurement, reframed as a within-subject trajectory, is not.

This reframing helped ALPS more than it helped MMSE. %MMSE change separated the two groups more cleanly, with a large rather than medium effect size (Cohen's d = 1.407, 95% CI: 0.794-2.021; Table 3.6), and only 10.0% of Stable MCI subjects showed MMSE decline as extreme as the MCI-to-AD group's median, against 19.4% for ALPS (Table 3.5). MMSE was already a fairly strong discriminator even at baseline, so there was less room for the change-score reframing to improve it. This asymmetry suggests the shift from baseline to change specifically rescues ALPS as a usable marker, rather than being a general improvement any variable would get from the same treatment.

Among the 52 subjects with both measures available, %ALPS change and %MMSE change were weakly and non-significantly correlated (Pearson r = 0.204, 95% CI: -0.073 to 0.452, p = 0.146; Spearman $\rho = 0.144$, p = 0.309; Table 3.7), indicating the two markers are not redundant. This is unlikely to reflect measurement unreliability. More plausibly, ALPS change and MMSE change capture partially separate components of conversion risk rather than one shared decline process. The weak correlation also works in the joint model's favour. Had the two predictors been strongly correlated, their shared significance in the combined logistic regression (Table 3.10) would be harder to trust, since collinearity can distort coefficients and inflate standard errors. Because the correlation is weak, that concern largely falls away.

The AUC and coefficient results measure different things, which is worth clarifying before interpreting them together. Under LOOCV, the combined model's AUC was statistically indistinguishable from %MMSE change alone and only modestly and non-significantly higher

than %ALPS change alone (0.654, 95% CI: 0.514-0.783; difference = 0.117, p = 0.14; Table S9). In practical terms, adding ALPS change to the model did not meaningfully improve its predictions beyond what MMSE change already provided.

Despite this, %ALPS change and %MMSE change both remained independently significant in the joint model (β_{ALPS} = -0.816, p = 0.045; β_{MMSE} = -1.618, p = 0.0006; Table 3.10). These findings are not actually inconsistent; they answer different questions. AUC measures how well a model ranks subjects by risk overall. A regression coefficient asks something narrower: once the MMSE change is already known, does the ALPS change provide additional information? A predictor can answer yes to the second question without meaningfully improving the first, particularly at this sample size, where the confidence intervals around AUC are wide relative to the differences being compared.

Practically, this means %ALPS change may currently be more useful as corroborating or mechanistic evidence than as something that sharpens a conversion-risk classifier already built on %MMSE change. That fits the underlying biology: glymphatic dysfunction is thought to be a distinct contributing pathway, not just a downstream echo of the same cognitive decline MMSE already tracks. Still, a weak standalone classifier is not the same claim as a weak biomarker. %ALPS change showed a medium effect size, discriminated converters from stable subjects better than chance on its own, and stayed significant even after MMSE was accounted for, three separate signs that this measure carries real information, even if it is not yet strong enough alone to justify use as a standalone diagnostic tool.

These findings sit naturally alongside Guo et al. (2025), who linked baseline ALPS to AD diagnosis using a support vector machine (AUC = 0.802 in an ADNI discovery cohort of N = 180, 0.783 in an independent validation cohort of N = 127), to future MMSE trajectory across the whole cohort (higher baseline ALPS associated with less decline, $\beta = 0.211$, $p < 0.001$), and to conversion risk via Cox regression (hazard ratio = 0.76 per 0.1-unit increase in baseline ALPS, 95% CI: 0.61-0.94, p = 0.014). Huang et al. (2024) reported a similar pattern in a separate ADNI sample, with baseline ALPS predicting later amyloid accumulation, brain atrophy, and cognitive decline, reinforcing that a baseline-predicts-future design is the field's dominant approach rather than a choice specific to Guo et al. (2025). This study instead asks whether change in ALPS and change in MMSE move together and jointly predict conversion, a trajectory-predicts-trajectory design. The distinction is about which question each design answers, not which one is better.

Where the two approaches diverge and where they agree is itself informative. Guo et al.'s (2025) correlation between baseline ALPS and baseline MMSE ($r = 0.283$, $p < 0.001$, N = 180; $r = 0.291$, $p < 0.01$, N = 127 in validation) was far more decisive than the %ALPS change-%MMSE change correlation reported here ($r = 0.204$, p = 0.146, N = 52). Sample size is the likeliest reason: their cohorts are three to four times larger, and a percentage-change measure drawn from two timepoints carries more compounded noise than a single baseline reading. Classification performance tells a different story. Guo et al.'s (2025) SVM reached an AUC of 0.802 in discovery and 0.783 in validation, close to the combined model's 0.809 here (Table S9). So, the two approaches don't diverge across the board: baseline measurements give more statistically decisive correlations at this sample size, largely a function of cohort size and measurement noise, while overall classification performance lands in a similar range for both.

The present study is best read as complementary to baseline-marker approaches like these, not a replacement for them; trajectory-based and baseline-based prediction are different, worthwhile questions, and the two may prove more informative together than either is alone. The %ALPS change finding fits the broader case that glymphatic dysfunction is a plausible upstream contributor to disease progression (Iliff et al., 2012; Kamagata, Andica, et al., 2022), though it doesn't establish that mechanism on its own (Ringstad, 2024). The medium effect size for %ALPS change (Cohen's d = 0.617; Table 3.6) is consistent with glymphatic decline contributing to, rather than single-handedly driving, the path from MCI to AD.

5. Limitations

The n = 52 subsample used for the combined-predictor and correlation analyses is modest for a two-predictor logistic regression; with 22 MCI-to-AD conversions among these 52 subjects (Table 3.4), that works out to roughly 11 events per predictor, close to the conventional rule-of-thumb minimum of 10. Confidence intervals throughout this subsample, for AUC, the correlation coefficients, and the joint-model odds ratios, are correspondingly wide and should be read as genuine estimation uncertainty rather than precise point estimates.

Because %ALPS change and %MMSE change are each computed from two separate timepoints, both inherit measurement error from both, which likely widens these intervals further and may partly explain why the change-based results here are less statistically decisive than the baseline-based results in Guo et al. (2025). Follow-up duration also varied across subjects, which is why we computed annualized as well as raw percentage change; even so, variation in the interval over which change is measured can introduce heterogeneity that annualization does not fully remove.

Subjects missing baseline or follow-up MMSE data (n = 16) did not differ significantly from complete cases on %ALPS change, annualized %ALPS change, or follow-up duration (all $p > 0.05$; Table 11), consistent with the missingness being unrelated to these measures. That comparison cannot rule out missingness tied to MMSE itself or to unmeasured factors, so the MMSE-based and combined results should be understood as applying to the subset of subjects with longitudinal MMSE data available, which may not fully represent the broader Stable MCI and MCI-to-AD population.

Reproducibility work on the ALPS index has found high test-retest reliability only under matched acquisition geometry (Taoka et al., 2022), and ADNI's multi-site, multi-scanner design means this condition may not hold uniformly across the present sample, a caveat for how confidently the observed variance in %ALPS change can be attributed to true biological change rather than site or scanner effects (Liu et al., 2023; Taoka et al., 2022). This analysis is also scoped to Stable MCI versus MCI-to-AD subjects specifically; the findings should not be assumed to generalize to CN-based trajectories or diagnostic reversal cases without separate testing. Unlike Guo et al.'s (2025) two-cohort design, this study uses ADNI data alone: the combined model has not been externally validated, and its LOOCV estimate, while a reasonable safeguard against overfitting, is not a substitute for testing on an independent cohort. Conversion status itself depends on the diagnostic criteria and follow-up window ADNI applies at each visit, which carries its own measurement uncertainty separate from the imaging and cognitive measures examined here.

6. Conclusions

The percentage change in the DTI-ALPS index from baseline, computed the same way as the percentage change in MMSE, distinguishes Stable MCI from MCI-to-AD subjects and adds independent information about conversion status even after accounting for MMSE change. This is a calibrated finding: it does not claim that ALPS change improves a classifier already built on MMSE change, only that it carries statistically independent information within the joint model reported here.

What this study set out to test is now supported by data rather than assumed: absolute baseline ALPS overlaps substantially across diagnostic groups, while change-from-baseline offers a cleaner, if still imperfect, separation between Stable MCI and MCI-to-AD. What is reported here is evidence of association and independent statistical contribution, not a validated clinical threshold or a classifier ready for individual-level prediction, and the wide confidence intervals, modest sample size, and lack of external validation together argue against treating these findings as a clinical decision tool at this stage.

7. Future Directions

These limitations point toward fairly concrete next steps. The most useful would be testing the combined model in an independent, prospectively followed cohort, which would let the classification and correlation estimates reported here be checked against a larger sample and narrow the wide intervals that come with n = 52. It would also be worth testing whether trajectory-based and baseline-based prediction work better together than either alone, by combining %ALPS change and %MMSE change with baseline predictors like those used by Guo et al. (2025) and Huang et al. (2024) in one model. A larger cohort would help on the diagnostic side, too. Subjects diagnosed with AD at baseline numbered only 13 here, separate from the larger group who converted to AD during follow-up, so a bigger baseline-AD sample would clarify how these markers behave once the disease is already established. Multi-shell diffusion scans, unavailable in this dataset, might also pick up glymphatic changes that standard single-shell DTI misses. On the pipeline side, the outlier threshold used to exclude subjects and the registration quality cutoff were set after looking at this data, rather than fixed in advance; future work would do better to decide these beforehand and check them against manually reviewed scans. Scanner field strength and acquisition settings also varied across the ADNI phases used here, so it would help to test directly whether %ALPS change holds up across scanners and protocols, either by including site as a variable or by validating the pipeline on already-harmonized data. Finally, since what this study shows is an association and an independent statistical contribution, not a confirmed biological mechanism, pairing %ALPS change with other glymphatic markers, CSF clearance measures or PET imaging would help establish whether it is picking up the same underlying process those methods measure.

Acknowledgements

The authors thank the Alzheimer's Disease Neuroimaging Initiative (ADNI) for providing the imaging and clinical data used in this study. The authors also acknowledge the School of Electrical Engineering, Manipal Institute of Technology, Manipal Academy of Higher Education, for institutional support, including access to computing resources and laboratory facilities used in this work.

The authors thank Psychological Assessment Resources, Inc. (PAR) for granting permission to use MMSE data in this publication (letter of permission dated 4 September 2026). The MMSE is a copyrighted instrument and may not be used or reproduced in whole or in part, in any form or language, or by any means without written permission of PAR (www.parinc.com).

Author Contributions

R.I. contributed to the DTI-ALPS computation pipeline, performed the diffusion imaging feature extraction, contributed to the methodological framework, conducted the statistical analysis, and wrote the original draft of the manuscript. H.S. contributed to the DTI-ALPS index computation and contributed to drafting the manuscript. A.G. conceived and designed the study, contributed to the methodological framework, supervised the statistical analysis, drafted portions of the manuscript, and reviewed and edited the final manuscript. All authors reviewed and approved the final manuscript.

Competing Interests

The authors declare no competing interests.

Funding

This research received no external funding.

Data Availability Statement

The data used in this study are available from the Alzheimer's Disease Neuroimaging Initiative (ADNI) database (https://adni.loni.usc.edu), subject to ADNI's standard data use agreement and application process. Derived subject-level variables generated during this study (DTI-ALPS index values, MMSE scores, and diagnostic trajectory classifications) are available from the corresponding author upon reasonable request, in accordance with ADNI's data sharing policies.

Ethics Declarations

This study used previously collected, de-identified data from the Alzheimer's Disease Neuroimaging Initiative (ADNI). Data collection procedures were approved by the Institutional Review Boards of all participating ADNI sites, and written informed consent was

obtained from all participants or their authorized representatives at the time of original data collection. No new human subject data were collected for this study.

References

Arani, A., Borowski, B., Felmlee, J., Reid, R. I., Thomas, D. L., Gunter, J. L., Stables, L., Buckner, R. L., Jung, Y., Tosun, D., Weiner, M., Jack, C. R., & for the Alzheimer's Disease Neuroimaging Initiative. (2024). Design and validation of the ADNI MR protocol. *Alzheimer's & Dementia*, *20*(9), 6615–6621. https://doi.org/10.1002/alz.14162

Bao, C., Luo, H., Wang, J., Liu, X., Li, Y., Yang, J., Chen, C., Yang, R., Ba, W., Lian, X., Dunk, M., Liu, J., & Xu, W. (2025). Poor glymphatic function is associated with mild cognitive impairment and its progression to Alzheimer's disease: A DTI-ALPS study. *The Journal of Prevention of Alzheimer's Disease*, *12*(7), 100156. https://doi.org/10.1016/j.tjpad.2025.100156

Basser, P. J., Mattiello, J., & LeBihan, D. (1994). MR diffusion tensor spectroscopy and imaging. *Biophysical Journal*, *66*(1), 259–267. https://doi.org/10.1016/S0006-3495(94)80775-1

Devanand, D. P., Liu, X., Tabert, M. H., Pradhaban, G., Cuasay, K., Bell, K., De Leon, M. J., Doty, R. L., Stern, Y., & Pelton, G. H. (2008). Combining Early Markers Strongly Predicts Conversion from Mild Cognitive Impairment to Alzheimer's Disease. *Biological Psychiatry*, *64*(10), 871–879. https://doi.org/10.1016/j.biopsych.2008.06.020

Devanand, D. P., Pradhaban, G., Liu, X., Khandji, A., De Santi, S., Segal, S., Rusinek, H., Pelton, G. H., Honig, L. S., Mayeux, R., Stern, Y., Tabert, M. H., & De Leon, M. J. (2007). Hippocampal and entorhinal atrophy in mild cognitive impairment: Prediction of Alzheimer disease. *Neurology*, *68*(11), 828–836. https://doi.org/10.1212/01.wnl.0000256697.20968.d7

Ewers, M., Walsh, C., Trojanowski, J. Q., Shaw, L. M., Petersen, R. C., Jack, C. R., Feldman, H. H., Bokde, A. L. W., Alexander, G. E., Scheltens, P., Vellas, B., Dubois, B., Weiner, M., & Hampel, H. (2012). Prediction of conversion from mild cognitive impairment to Alzheimer's disease dementia based upon biomarkers and neuropsychological test performance. *Neurobiology of Aging*, *33*(7), 1203-1214.e2. https://doi.org/10.1016/j.neurobiolaging.2010.10.019

Folstein, M. F., Folstein, S. E., & McHugh, P. R. (1975). "Mini-mental state." *Journal of Psychiatric Research*, *12*(3), 189–198. https://doi.org/10.1016/0022-3956(75)90026-6

Garyfallidis, E., Brett, M., Amirbekian, B., Rokem, A., Van Der Walt, S., Descoteaux, M., Nimmo-Smith, I., & Dipy Contributors. (2014). Dipy, a library for the analysis of diffusion MRI data. *Frontiers in Neuroinformatics*, *8*. https://doi.org/10.3389/fninf.2014.00008

Gomar, J. J. (2011). Utility of Combinations of Biomarkers, Cognitive Markers, and Risk Factors to Predict Conversion From Mild Cognitive Impairment to Alzheimer Disease in Patients in the Alzheimer's Disease Neuroimaging Initiative. *Archives of General Psychiatry*, *68*(9), 961. https://doi.org/10.1001/archgenpsychiatry.2011.96

Guo, Y., Liu, T., Chen, H., Zhou, L., Huang, W., Zhang, K., Wang, X., Wang, Y., Zhou, J. H., & Chen, F. (2025). Decreased brain interstitial fluid dynamics is associated with risk of Alzheimer's disease-related cognitive decline. *Brain Research Bulletin*, *224*, 111295. https://doi.org/10.1016/j.brainresbull.2025.111295

Huang, S., Zhang, Y., Guo, Y., Du, J., Ren, P., Wu, B., Feng, J., Alzheimer's Disease Neuroimaging Initiative, Cheng, W., & Yu, J. (2024). Glymphatic system dysfunction predicts amyloid deposition, neurodegeneration, and clinical progression in Alzheimer's disease. *Alzheimer's & Dementia*, *20*(5), 3251–3269. https://doi.org/10.1002/alz.13789

Iliff, J. J., Lee, H., Yu, M., Feng, T., Logan, J., Nedergaard, M., & Benveniste, H. (2013). Brain-wide pathway for waste clearance captured by contrast-enhanced MRI. *Journal of Clinical Investigation*, *123*(3), 1299–1309. https://doi.org/10.1172/JCI67677

Iliff, J. J., Wang, M., Liao, Y., Plogg, B. A., Peng, W., Gundersen, G. A., Benveniste, H., Vates, G. E., Deane, R., Goldman, S. A., Nagelhus, E. A., & Nedergaard, M. (2012). A Paravascular Pathway Facilitates CSF Flow Through the Brain Parenchyma and the Clearance of Interstitial Solutes, Including Amyloid β. *Science Translational Medicine*, *4*(147). https://doi.org/10.1126/scitranslmed.3003748

Jack, C. R., Bernstein, M. A., Fox, N. C., Thompson, P., Alexander, G., Harvey, D., Borowski, B., Britson, P. J., L. Whitwell, J., Ward, C., Dale, A. M., Felmlee, J. P., Gunter, J. L., Hill, D. L. G., Killiany, R., Schuff, N., Fox-Bosetti, S., Lin, C., Studholme, C., … Weiner, M. W. (2008). The Alzheimer's disease neuroimaging initiative (ADNI): MRI methods. *Journal of Magnetic Resonance Imaging*, *27*(4), 685–691. https://doi.org/10.1002/jmri.21049

Kamagata, K., Takabayashi, K., Saito, Y., Taoka, T., Nozaki, H., Kikuta, J., Fujita, S., Hagiwara, A., Kamiya, K., Wada, A., Akashi, T., Sano, K., Nishizawa, M., Hori, M., Naganawa, S., Aoki, S., & for the Alzheimer's Disease Neuroimaging Initiative. (2022). Association of MRI Indices of Glymphatic System With Amyloid Deposition and Cognition in Mild Cognitive Impairment and Alzheimer Disease. *Neurology*, *99*(24). https://doi.org/10.1212/WNL.0000000000201300

Liu, X., Barisano, G., Shao, X., Jann, K., Ringman, J. M., Lu, H., Arfanakis, K., Caprihan, A., DeCarli, C., Gold, B. T., Maillard, P., Satizabal, C. L., Fadaee, E., Habes, M., Stables, L., Singh, H., Fischl, B., Kouwe, A. V. D., Schwab, K., … Wang, D. J. J. (2023). Cross-Vendor Test-Retest Validation of Diffusion Tensor Image Analysis along the Perivascular Space (DTI-ALPS) for Evaluating Glymphatic System Function. *Aging and Disease*, 0. https://doi.org/10.14336/AD.2023.0321-2

Nakaya, M., Kamagata, K., Takabayashi, K., Andica, C., Uchida, W., Hagiwara, A., Akashi, T., Wada, A., Taoka, T., Naganawa, S., Abe, O., & Aoki, S. (2025). *Magnetic resonance imaging indices for early Alzheimer's disease detection: Brain clearance markers*.

Nedergaard, M., & Goldman, S. A. (2020). Glymphatic failure as a final common pathway to dementia. *Science*, *370*(6512), 50–56. https://doi.org/10.1126/science.abb8739

Nichols, E., Steinmetz, J. D., Vollset, S. E., Fukutaki, K., Chalek, J., Abd-Allah, F., Abdoli, A., Abualhasan, A., Abu-Gharbieh, E., Akram, T. T., Al Hamad, H., Alahdab, F., Alanezi, F. M., Alipour, V., Almustanyir, S., Amu, H., Ansari, I., Arabloo, J., Ashraf, T., … Vos, T. (2022). Estimation of the global prevalence of dementia in 2019 and forecasted prevalence in 2050: An analysis for the Global Burden of Disease Study 2019. *The Lancet Public Health*, *7*(2), e105–e125. https://doi.org/10.1016/S2468-2667(21)00249-8

Petersen, R. C., Aisen, P. S., Beckett, L. A., Donohue, M. C., Gamst, A. C., Harvey, D. J., Jack, C. R., Jagust, W. J., Shaw, L. M., Toga, A. W., Trojanowski, J. Q., & Weiner, M. W. (2010). Alzheimer's Disease Neuroimaging Initiative (ADNI): Clinical characterization. *Neurology*, *74*(3), 201–209. https://doi.org/10.1212/WNL.0b013e3181cb3e25

Ringstad, G. (2024). Glymphatic imaging: A critical look at the DTI-ALPS index. *Neuroradiology*, *66*(2), 157–160. https://doi.org/10.1007/s00234-023-03270-2

Stejskal, E. O., & Tanner, J. E. (1965). Spin Diffusion Measurements: Spin Echoes in the Presence of a Time-Dependent Field Gradient. *The Journal of Chemical Physics*, *42*(1), 288–292. https://doi.org/10.1063/1.1695690

Steward, C. E., Venkatraman, V. K., Lui, E., Malpas, C. B., Ellis, K. A., Cyarto, E. V., Vivash, L., O'Brien, T. J., Velakoulis, D., Ames, D., Masters, C. L., Lautenschlager, N. T., Bammer, R., & Desmond, P. M. (2021). Assessment of the DTI-ALPS Parameter Along the Perivascular Space in Older Adults at Risk of Dementia. *Journal of Neuroimaging*, *31*(3), 569–578. https://doi.org/10.1111/jon.12837

Taoka, T., Ito, R., Nakamichi, R., Kamagata, K., Sakai, M., Kawai, H., Nakane, T., Abe, T., Ichikawa, K., Kikuta, J., Aoki, S., & Naganawa, S. (2022). Reproducibility of diffusion tensor image analysis along the perivascular space (DTI-ALPS) for evaluating interstitial fluid diffusivity and glymphatic function: CHanges in Alps index on Multiple conditiON acquIsition eXperiment (CHAMONIX) study. *Japanese Journal of Radiology*, *40*(2), 147–158. https://doi.org/10.1007/s11604-021-01187-5

Taoka, T., Masutani, Y., Kawai, H., Nakane, T., Matsuoka, K., Yasuno, F., Kishimoto, T., & Naganawa, S. (2017). Evaluation of glymphatic system activity with the diffusion MR technique: Diffusion tensor image analysis along the perivascular space (DTI-ALPS) in Alzheimer's disease cases. *Japanese Journal of Radiology*, *35*(4), 172–178. https://doi.org/10.1007/s11604-017-0617-z

Virtanen, P., Gommers, R., Oliphant, T. E., Haberland, M., Reddy, T., Cournapeau, D., Burovski, E., Peterson, P., Weckesser, W., Bright, J., Van Der Walt, S. J., Brett, M., Wilson, J., Millman, K. J., Mayorov, N., Nelson, A. R. J., Jones, E., Kern, R., Larson, E., … Vázquez-Baeza, Y. (2020). SciPy 1.0: Fundamental algorithms for scientific computing in Python. *Nature Methods*, *17*(3), 261–272. https://doi.org/10.1038/s41592-019-0686-2

Weiner, M. W., Veitch, D. P., Aisen, P. S., Beckett, L. A., Cairns, N. J., Green, R. C., Harvey, D., Jack, C. R., Jagust, W., Morris, J. C., Petersen, R. C., Salazar, J., Saykin, A. J., Shaw,

L. M., Toga, A. W., Trojanowski, J. Q., & Alzheimer's Disease Neuroimaging Initiative. (2017). The Alzheimer's Disease Neuroimaging Initiative 3: Continued innovation for clinical trial improvement. *Alzheimer's & Dementia*, *13*(5), 561–571. https://doi.org/10.1016/j.jalz.2016.10.006

Xie, L., Kang, H., Xu, Q., Chen, M. J., Liao, Y., Thiyagarajan, M., O'Donnell, J., Christensen, D. J., Nicholson, C., Iliff, J. J., Takano, T., Deane, R., & Nedergaard, M. (2013). Sleep Drives Metabolite Clearance from the Adult Brain. *Science*, *342*(6156), 373–377. https://doi.org/10.1126/science.1241224

Zhang, W., Zhou, Y., Wang, J., Gong, X., Chen, Z., Zhang, X., Cai, J., Chen, S., Fang, L., Sun, J., & Lou, M. (2021). Glymphatic clearance function in patients with cerebral small vessel disease. *NeuroImage*, *238*, 118257. https://doi.org/10.1016/j.neuroimage.2021.118257

Supplementary Files

This is a list of supplementary files associated with this preprint. Click to download.

- SupplementaryMaterialIngavaleetal2026RevisedSept282026.docx